Contents lists available at ScienceDirect

Chemical Engineering Research and Design

journal homepage: www.elsevier.com/locate/cherd

Resolving the rapid water absorption of porous functionalised calcium carbonate powder compacts by terahertz pulsed imaging

Daniel Markl[a,*], *Parry Wang*[a], *Cathy Ridgway*[b], *Anssi-Pekka Karttunen*[c], *Prince Bawuah*[c], *Jarkko Ketolainen*[c], *Patrick Gane*[b,e], *Kai-Erik Peiponen*[d], *J. Axel Zeitler*[a]

[a] *Department of Chemical Engineering and Biotechnology, University of Cambridge, Philippa Fawcett Drive, CB3 0AS Cambridge, UK*
[b] *Omya International AG, 4665 Oftringen, Switzerland*
[c] *School of Pharmacy, Promis Centre, University of Eastern Finland, P.O. Box 1617, 70211 Kuopio, Finland*
[d] *Institute of Photonics, University of Eastern Finland, P.O. Box 111, 80101 Joensuu, Finland*
[e] *School of Chemical Engineering, Department of Bioproducts and Biosystems, Aalto University, P.O. Box 11000, 00076 Aalto, Finland*

ARTICLE INFO

Article history:
Received 3 August 2017
Received in revised form 30 November 2017
Accepted 28 December 2017
Available online 5 January 2018

Keywords:
Porous media
Pharmaceutical tablets
Functionalised calcium carbonate
Terahertz pulsed imaging
Liquid imbibition
Modelling

ABSTRACT

Cost effectiveness, ease of use and patient compliance make pharmaceutical tablets the most popular and widespread form to administer a drug to a patient. Tablets typically consist of an active pharmaceutical ingredient and a selection from various excipients. A novel highly porous excipient, functionalised calcium carbonate (FCC), was designed to facilitate rapid liquid uptake leading to disintegration times of FCC based tablets in the matter of seconds. Five sets of FCC tablets with a target porosity of 45–65% in 5% steps were prepared and characterised using terahertz pulsed imaging (TPI). The high acquisition rate (15 Hz) of TPI enabled the analysis of the rapid liquid imbibition of water into these powder compacts. The penetration depth determined from the TPI measurements as a function of time was analysed by the power law and modelled for both the inertial (initial phase) and Lucas-Washburn (LW, longer time Laplace- Poiseuillian) regimes. The analysis of the hydraulic radius estimated by fitting the liquid imbibition data to the LW equation demonstrates the impact of the porosity as well as the tortuosity of the pore channels on the liquid uptake performance. The tortuosity was related to the porosity by a geometrical model, which shows that the powder compact is constructed by aggregated particles with low permeability and its principal axis perpendicular to the compaction direction. The consideration of the tortuosity yielded a very high correlation ($R^2 = 0.96$) between the porosity and the hydraulic pore radius. The terahertz data also resolved fluctuations (0.9–1.3 Hz) of the liquid movement which become more pronounced and higher in frequency with increasing porosity, which is attributed to the constrictivity of pore channels. This study highlights the strong impact of a tablet's microstructure on its liquid penetration kinetics and thus on its disintegration behaviour.

* *Corresponding author.*
E-mail address: dm733@cam.ac.uk (D. Markl).
https://doi.org/10.1016/j.cherd.2017.12.048

1. Introduction

Pharmaceutical tablets are well-known as being amongst the most convenient ways of delivering active pharmaceutical ingredient (API) to the patient. Tablets are typically manufactured via powder compaction and consist of API particles and a selection of various excipients. The physical and chemical properties of both API and excipient particles dominate tableting and delivery functionality of the dosage form. However, in most cases the excipients represent by far the greater quantity in a tablet and, therefore, it is not surprising that they play a crucial role in defining the ease of tableting generally in respect to material flow, compressibility and compaction. Increasingly, the design of targeted drug release and vector delivery requires specialist development of functional excipients, for example, to encapsulate an API to provide protective access into the small and large intestine or to provide rapid oral disintegration.

In particular, the performance of orally disintegrating tablets (ODTs) is strongly impacted by the pore structure of the excipients and the overall microstructure of the tablet. ODTs are designed to disintegrate rapidly, usually in the matter of seconds, in the mouth which facilitates easy administration and convenience. About 35% of the general population suffer from difficulties in swallowing (Sastry et al., 2000), and for these patients in particular ODTs provide a significant improvement in therapy. Once in the mouth, saliva penetrates the dosage form and even a small amount of 1–2 mL should be sufficient to achieve disintegration. The performance of an ODT is limited by the rate saliva penetrates into the tablet leading to swelling of the (superdisintegrant) particles and eventually causing the break-up of the compact into small agglomerates or the original constituents' particles. The understanding of this process is severely limited, partly due to the complex nature of the process itself and partly due to the lack of suitable measurement techniques. The conventional disintegration apparatus and testing procedures described by the pharmacopoeia are not suitable to assess the performance of such rapidly disintegrating tablets quantitatively. Hence, alternative methods to measure rapid disintegration are highly desirable to evaluate ODTs and to control the quality of such drug products.

Liquid uptake of and penetration into powder compacts have been studied by a range of approaches (Quodbach and Kleinebudde, 2016; Desai et al., 2016; Markl and Zeitler, 2017). Several studies were performed to measure the water uptake into powder beds and into powder compacts using an optical camera (Hapgood et al., 2002; Nguyen et al., 2009; Desai et al., 2012), gravimetric techniques (Nogami et al., 1966; Caramella et al., 1986; Catellani et al., 1989; Peppas and Colombo, 1989; Esteban et al., 2017) or magnetic resonance imaging (MRI) (Tritt-Goc and Kowalczuk, 2002; Nott, 2010; Quodbach et al., 2014). Another technology to resolve the structure of pharmaceutical tablets is X-ray computed microtomography (XμCT) (Wildenschild and Sheppard, 2013). MRI and XμCT are superior compared to an optical camera or gravimetric techniques as they allow to resolve the internal structure of porous materials in a non-destructive and contactless manner. However, the drawback of both methods is their long measurement time ($\gg$1 min), which renders them unsuitable to study the liquid imbibition into highly-porous media that fully hydrate within seconds. A very promising tool to analyse such rapid liquid penetration kinetics is terahertz pulsed imaging (TPI). Yassin et al. (2015) coupled a TPI with a flow cell to study liquid imbibition and swelling of various microcrystalline cellulose (MCC) based immediate-release formulations. These studies emphasised the impact of the porosity on the disintegration performance of such tablets. The porosity of pharmaceutical tablets can be measured using terahertz technology in a transmission setting. Bawuah et al. (2016) measured tablets consisting of pure MCC and combined with an API by terahertz time-domain spectroscopy (THz-TDS) to determine the effective refractive index and, thereby, the porosity. It was also demonstrated that this method works for biconvex tablets as well as for complex formulations (Markl et al., 2017a).

Table 1 – List of the five batches characterised in this study. The presented data slightly differ from the data in Markl et al. (2017b) as only a subset of the batch was used in this study. Batches B01 and B05 consisting of 5 tablets, and 6 tablets were measured for the batches B02-B04. The porosities were determined by THz-TDS in combination with the anisotropic Bruggeman model.

Batch	Diameter (mm)	Thickness, L (mm)	Mass (mg)	Porosity, f (%)
B01	10.04	1.67	216 ± 2	46.2 ± 0.3
B02	10.03	1.64	190 ± 2	51.8 ± 0.5
B03	10.02	1.63	168 ± 2	56.6 ± 0.3
B04	10.03	1.62	146 ± 4	62.0 ± 0.4
B05	10.00	1.61	125 ± 2	67.3 ± 0.4

A highly viable excipient for ODT formulations is functionalised calcium carbonate (FCC), which has a high intra-particle porosity (Stirnimann et al., 2013). FCC based tablets have a discretely separable bimodal pore size distribution, consisting of large inter-particle and fine intra-particle pores (Markl et al., 2017b). The inter-particle pores are formed during the powder compaction and therefore, they can be modified by adjusting the compaction process.

In this study we investigated the interaction of the pore structure of FCC tablets with liquid during imbibition. The *in-situ* monitoring approach by means of terahertz technology was further developed to study the rapid imbibition of the FCC tablets. The imbibition process was analysed and modelled on the basis of the TPI data and it was related to the pore structure properties of the same tablets determined by THz-TDS (Markl et al., 2017b).

2. Materials and methods

2.1. Materials

Five batches of pure flat-faced FCC tablets were compacted to target porosities ranging from 45% to 65% with 5% increments (Table 1). The diameter and thickness of the tablets were kept constant at 10 mm and 1.5 mm, respectively, by varying the material weight. The pore structure of these FCC tablets was characterised by Markl et al. (2017b) using mercury porosimetry, XμCT and THz-TDS. Since XμCT and THz-TDS are non-destructive techniques, the tablets were still intact after the measurement and were used in this study. This facilitates the direct correlation of the results from this study with that from Markl et al. (2017b).

In general, FCC is formed in a process whereby the surface of micrometre sized calcium carbonate particles is etched and then re-precipitated to create a highly porous, high surface area material. The naming of the FCC material refers to the functionalisation of calcium carbonate as being the formation of highly-porous particles using a surface modification to form hydroxyapatite. A typical FCC entering use as

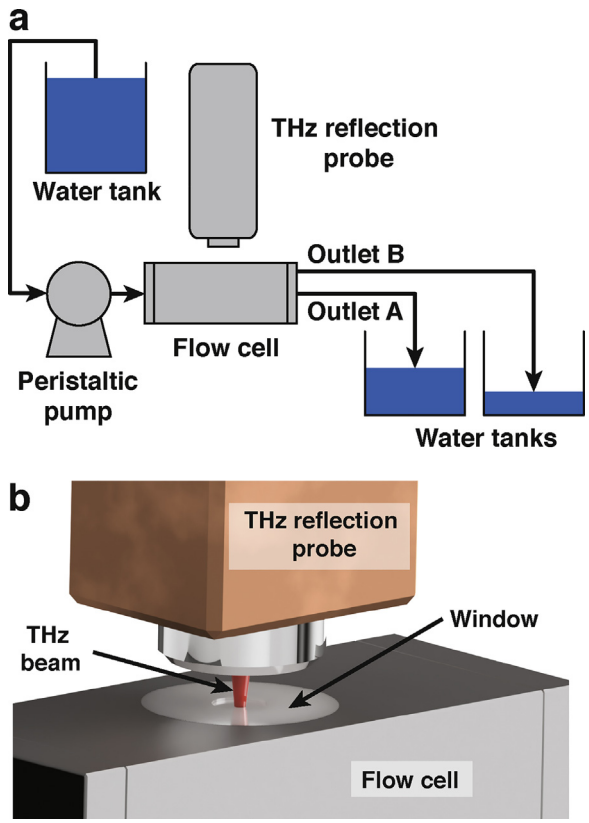

Fig. 1 – Experimental setup of the TPI coupled with a flow cell. (a) Schematic representation of the flow loop. (b) 3D visualisation of the terahertz reflection probe and the flow cell. The flow cell has a size of 10 cm × 5 cm × 5 cm. More details about the flow cell are provided by Yassin et al. (2015).

excipient (Omyapharm®, Omya International AG) consists of a calcium carbonate/hydroxyapatite structure, in which the plate-like nano-thickness lamellae of the phosphate component construct a network of fine pores on the surface and interior of the FCC particle.

2.2. *Terahertz pulsed imaging*

A commercial terahertz system (TeraPulse 4000, TeraView Ltd, Cambridge, UK) was coupled with a flow cell to monitor the hydration process of pharmaceutical tablets. The terahertz measurements were performed with a reflection probe equipped with an 18 mm focal length lens. The acquisition rate was set to 15 Hz and every measurement covered an optical delay of 38.8 ps.

The flow cell previously developed and utilised by Yassin et al. (2015) was optimised to enhance the accuracy of the measurements at the beginning of the hydration process. The tablet sits in a sample holder where it is exposed to the liquid on only one face (Fig. 1). The surface area of the tablet exposed to the liquid was $A_{wet} = 48.4\,mm^2$. The flow in the cell was controlled by valves at the inlet and the two outlets. The flow cell was sealed with a polyethylene window (PE), which is almost completely transparent to terahertz radiation.

The experiment was started with an open inlet valve and an open valve at outlet A. The experiments were carried out with water at 22.5 °C, which was the temperature in the water tank as well as at the outlet valve of the flow cell. The water was pumped at a flow rate of 13 mL/min using a peristaltic pump (530SN, Watson-Marlow Ltd, Falmouth, UK), which was equipped with a low-pulse pump head (505L, Watson-Marlow Ltd, Falmouth, UK). This pump head was specifically designed to provide a smooth flow and to minimise pressure fluctuations. The presence of an air bubble at the top of the cell prevented water from touching the tablet and therefore, the hydration process of a tablet was started by opening the valve at outlet B and simultaneously closing the valve at outlet A. The outlet B is located at the very top of the cell in order to release the air in the cell completely and to assure continuous wetting of the tablet.

The data acquisition was started at the same time when outlet B was opened. The water then slowly approached the tablet as it can be observed in the terahertz waveforms in Fig. 2. The water penetrating the powder compact changes the refractive index of the wetted material and thus enables the tracking of the penetration front (transient from wetted to dry material) by means of terahertz reflection technology. TPI thus facilitates the assessment of the one-dimensional transport of water into the tablet. The water front was automatically detected by a custom-built code using Matlab (MathWorks). Prior to tracking the liquid front, the measured terahertz waveforms were deconvolved to reduce the noise and enhance the peaks originating from the interfaces, i.e. air/dry tablet, dry tablet/air, and dry tablet/wet tablet). In general, the measured terahertz signal is a convolution of the input signal from the terahertz emitter and the impulse response of the sample as well as additive noise. The objective of a terahertz reflection measurement is to obtain the impulse response of the sample. This can be achieved by deconvolving the measured terahertz waveform and a reference measurement (a terahertz waveform of a mirror). However, it is well-known that this kind of inverse filtering amplifies high frequency noise, which is commonly suppressed by coupling the deconvolution and an appropriate band-pass filter. A double Gaussian filter was applied in this study:

$$f_{DG} = \frac{1}{HF}\exp\left(-\frac{t^2}{HF^2}\right) - \frac{1}{LF}\exp\left(-\frac{t^2}{LF^2}\right) \quad (1)$$

where HF and LF define the pulse width in respect to the high frequency and low frequency bounds of the band-pass filter, respectively.

3. Results and discussion

3.1. *Liquid imbibition*

The kinetics of the liquid imbibition process is strongly impacted by the pore structure in the powder compact (Fig. 3). Since the intra-particle pore structure of the FCC particles is similar between the different batches (Markl et al., 2017b), the variations in liquid uptake kinetics of the different batches are primarily affected by the inter-particle pore architecture which was formed during powder compaction. The absorption behaviour depends on the pore size distribution and the pore connectivity amongst other factors such as pore network geometry and surface energy. The observed correlation between porosity and liquid imbibition kinetics thus suggests that each powder compact is an homologous series of structures, in that the features of connectivity and pore size distribution remain related to porosity, i.e. the basic descriptors of the pore structure remain constant or vary continuously in line with the varied tablet compression.

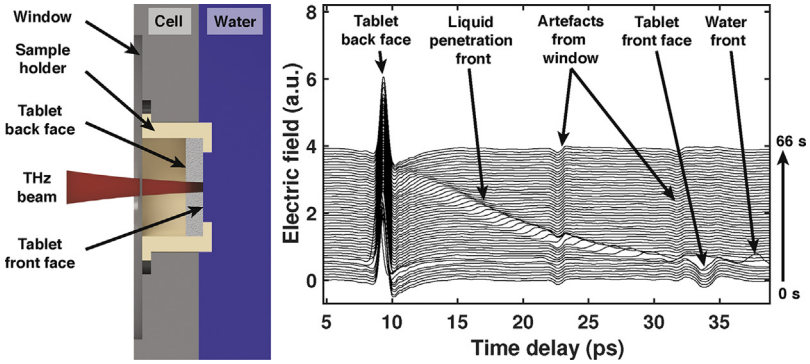

Fig. 2 – Schematic of the setup and deconvolved terahertz waveforms (each waveform is offset by 0.004 a.u.) showing the hydration of a tablet from batch B03.

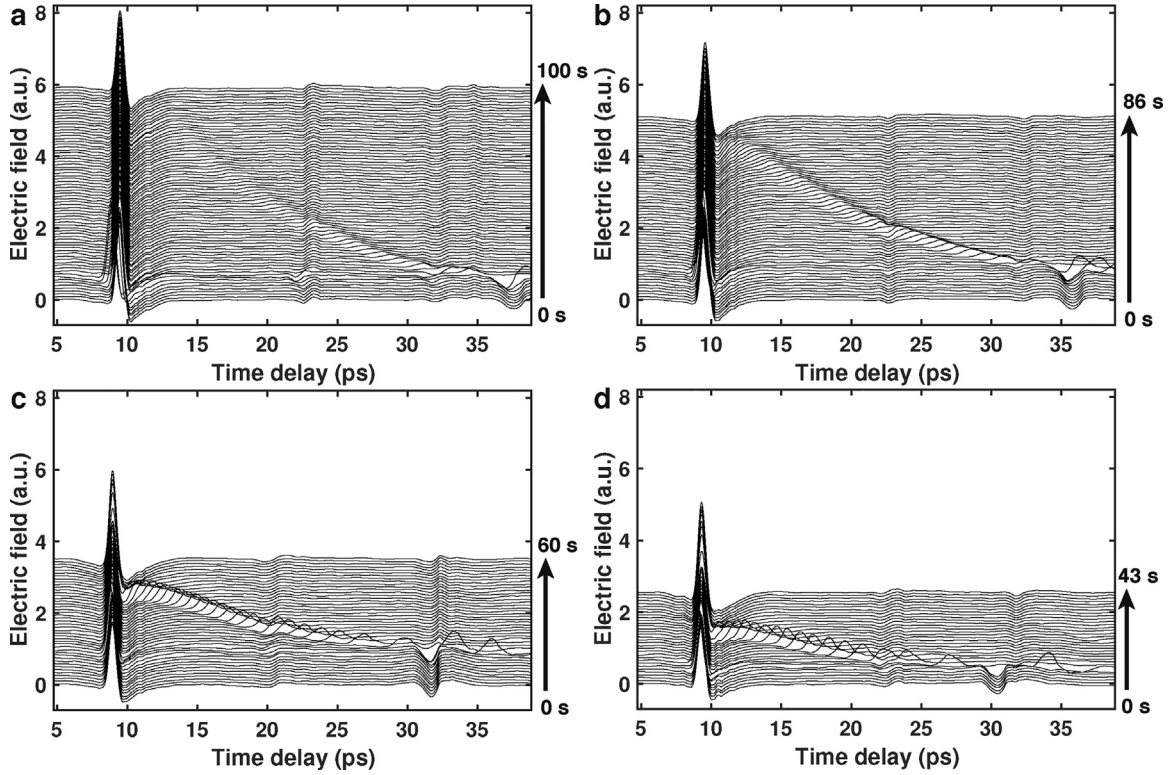

Fig. 3 – Deconvolved terahertz waveforms of one tablet per batch (each waveform is offset by 0.004 a.u.). (a) B01, (b) B02, (c) B04 and (d) B05. B03 is shown in Fig. 2.

As tablet porosity increases from batch B01 to B05, there is a decrease in the total duration for the tablet to become fully hydrated. The magnitude of the amplitude of the water front reflection is governed by the relative difference in refractive indices between the dry and wetted material. The measured amplitude is directly proportional to the reflection coefficient (Verdet convention (Holm, 1991)), which is defined as

$$r_{dw} = \frac{n_w - n_d}{n_w + n_d} \tag{2}$$

where n_d and n_w are the refractive indices of the dry and wetted material in the tablet, respectively. In general, the reflection coefficient and the refractive index of a porous medium are complex numbers. This is particularly important for materials which strongly absorb terahertz radiation. Markl et al. (2017b) presented the effective refractive index and absorption coefficient at terahertz frequencies. The absence of any features in the absorption coefficient indicated the absence of phonon vibrations. They also discussed that even though the calcium carbonate is birefringent as a single crystal (Mizuno et al., 2009), the random orientation of the calcium carbonate domains in an FCC particle and of the FCC particle in the powder compact renders birefringence immeasurably small.

Eq. (2) reveals that the reflected pulse can be either negative or positive depending on the relative change in refractive indices of the two media. The initial reflection is negative as the terahertz beam traverses from the dry FCC tablet to air ($n = 1$). However, the sign changes when the tablet comes in contact with water. The refractive index of water at 1 THz is ≈2.4 (Pickwell et al., 2004) and that of the dry material is equal to the effective refractive index, n_{eff}, of the FCC tablets as given in Markl et al. (2017b). n_{eff} ranges from 1.61 to 2.19 (high to low porosity) and therefore it is smaller than the refractive index of water causing a positive reflection peak at the water front. Since the relative difference between n_{eff} and the refractive index of water decreases with decreasing porosity, the amplitude of the reflection peak significantly drops for tablets from batch B05 (Fig. 3d) compared to those from batch B01 (Fig. 3a).

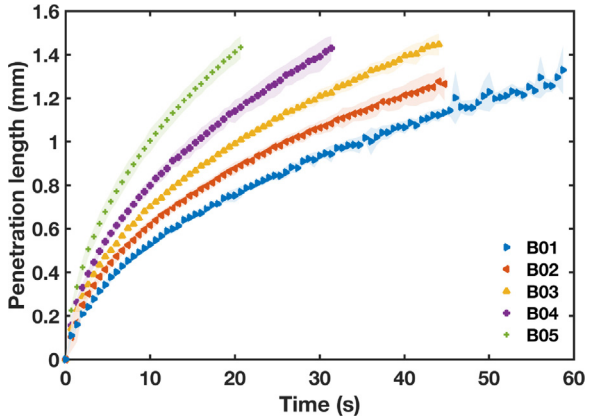

Fig. 4 – Penetration length (distance travelled by the liquid front) as a function of time. The average porosity of the tablets from the batches B01-B05 was 46.2%, 51.8%, 56.6%, 62.0% and 67.3%, respectively. Only every 10th data point is displayed and the shaded area corresponds to the standard deviation within each batch.

Since FCC particles are non-swelling and non-dissolving in water, pure FCC powder compacts do not disintegrate. This could also be observed in the terahertz measurements as the back face of the tablet (Fig. 3) did not move during the experiment and the powder compacts did not change their shape and microstructure after drying the hydrated tablets again. The results clearly demonstrate that the highly porous FCC powder was specifically designed to enhance the liquid uptake of pharmaceutical tablets (Stirnimann et al., 2013, 2014; Preisig et al., 2014; Wagner-Hattler et al., 2017; Eberle et al., 2015, 2014). The water penetration kinetics are strongly driven by the porosity of the tablets (Fig. 4). The small standard deviation reflects that the penetration kinetics are highly consistent within each batch.

FCC in combination with a superdisintegrant (Stirnimann et al., 2013), which primarily drives the swelling and thus builds up an internal stress, facilitates the design of a desired disintegration behaviour as each excipient imparts only one disintegration mechanism at a time. A design of a formulation based on a mechanistic understanding is more complex with excipients, such as MCC, impacting on disintegration via several mechanisms, which hamper the decoupling of the swelling and the liquid uptake. Mechanistic understanding can be reflected by models which describe swelling and liquid uptake (Markl et al., 2017c) as well as the break-up of the tablet. Modelling the different processes involved in disintegration independently would simplify the design significantly and this could eventually lead to models of commercial formulations which predict the disintegration behaviour, and this is facilitated by considering the ability to decouple absorption and swelling by using FCC as the sole absorption-promoting component.

The rate uptake into porous systems is typically described by the Lucas-Washburn (LW) equation, which combines the Laplace and the Hagen-Poiseuille equation and assumes that the pores are uniform and cylindrical. The penetration length, y, as a function of time t can thus be expressed for a laminar flow as

$$y(t) = \sqrt{\frac{R_{h,eq}\gamma\cos\theta t}{2\eta}} \quad (3)$$

Table 2 – Summary of the parameters fitted to the penetration data. The changeover, y_c, is the penetration length at which the kinetics change from inertial ($y < y_c$) to Laplace-Poiseuillian ($y \geq y_c$) flow regimes. This table lists only the average and standard deviation of the fitting parameters of the power law ($y = kt^m$) and the LW equation (Eq. (3)). The values for each fit are provided in Figs. 6 and 7.

Batch	y_c (μm)	k (mm s^{-m})	m	$R_{h,eq}$ (nm)
B01	109	0.16 ± 0.01	0.51± 0.02	1.16 ± 0.05
B02	104	0.20 ± 0.02	0.50± 0.02	1.50 ± 0.11
B03	145	0.22 ± 0.01	0.50± 0.02	1.95 ± 0.09
B04	163	0.24 ± 0.02	0.52± 0.03	2.61 ± 0.21
B05	240	0.31 ± 0.03	0.51± 0.01	4.02 ± 0.31

where θ is the contact angle between the water and the FCC component solid material in the powder compact, η is the dynamic viscosity of water and γ is the surface tension of water. The hydraulic radius, $R_{h,eq}$, is defined as the ratio between the pore volume to the solid-fluid interfacial area. We propose to account for the flow-dependent geometrical variables in the definition of the hydraulic radius by considering the tortuosity, $T = L_e/L$. T is a dimensionless number relating the average length of the fluid path, L_e, and the geometrical length of the sample (tablet thickness), L. The equivalent hydraulic radius as a function of the tortuosity (Shin, 2017) can be expressed as (see Appendix A for derivation)

$$R_{h,eq} = R_h T^{-1} = a\frac{f}{(1-f)}T^{-1}. \quad (4)$$

R_h as a function of porosity, f, was defined by Carman and Kozeny under the consideration of a shape factor, a (Nakayama et al., 2007).

In contrast to $y \propto \sqrt{t}$ as described by the LW equation (henceforth referred to as the Laplace-Poiseuillian flow regime), it is known that the liquid uptake length in compacted calcium carbonate is directly proportional to t for short timescales of the imbibition (henceforth referred to as the inertial flow regime). Schoelkopf et al. (2000) used the Bosanquet equation to consider both inertial and viscous forces acting on the liquid. The authors demonstrated that the liquid uptake length of compacted calcium carbonate blocks changes from a linear t-dependence to a $\sqrt{t}$-dependence. We also observe this change here in the measurements of the penetration length from the TPI data. The changeover, y_c, from the inertial to the Laplace-Poiseuillian flow regime was determined by minimising the root-mean-squared error (RMSE) of the measured penetration length against a fitting model expressed as

$$y(t) = \begin{cases} at + d, & \text{if } y < y_c \\ kt^m, & \text{otherwise.} \end{cases} \quad (5)$$

Eq. (5) consists of a linear equation and a power law with a, d, k and m as fitting parameters. y_c was determined for every batch and the values in Table 2 reveal that the changeover is at larger penetration lengths for higher porosity batches. This is in line with the observations in Schoelkopf et al. (2000), where the changeover was at a larger penetration length for tubes with larger radii. The initial penetration rate in the inertial flow regime scales linearly with the porosity (Fig. 5).

The power law was fitted to the data from the Laplace-Poiseuillian flow regime (Fig. 6). The fitted parameter k correlates linearly with the porosity and the exponent m indi-

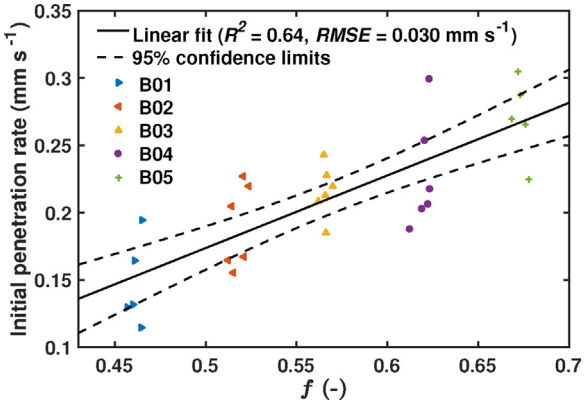

Fig. 5 – Initial penetration rate (a in Eq. (5)) as a function of the porosity. This parameter was determined from the data of the inertial flow regime ($y < y_c$).

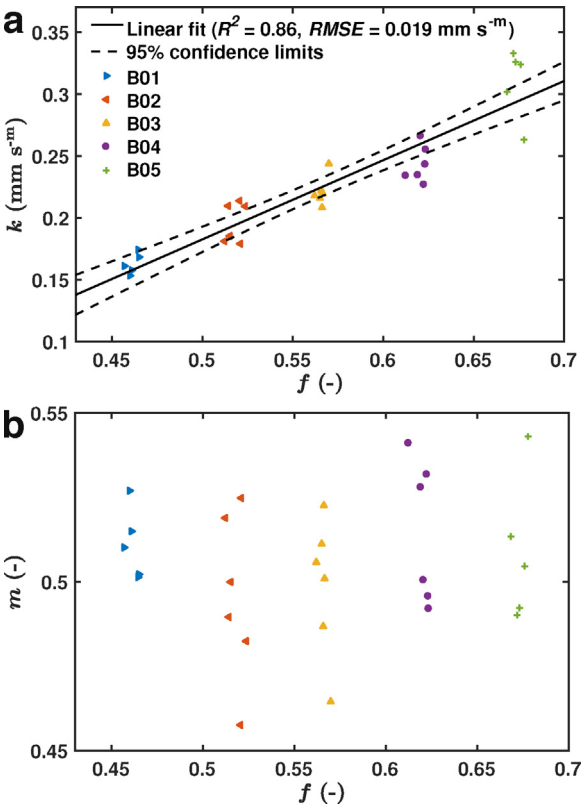

Fig. 6 – Fitting parameters of the power law (Eq. (5)) as a function of the porosity using the data from the Laplace-Poiseuillian ($y \geq y_c$) flow regime.

cates that the liquid penetration length is proportional to $\sqrt{t}$. This supports the use of the LW equation to determine the equivalent hydraulic radius of the powder compacts. The LW equation was fitted to the data in the Laplace-Poiseuillian flow regime of every measurement using $\gamma = 72.75\,\mathrm{N\,mm^{-1}}$ and $\eta = 1.002\,\mathrm{mPa\,s}$ of water and a contact angle of water-FCC of 46.7° (Koivula et al., 2011). We used the contact angle of calcite as the initial advancing and receding contact angles of calcite and hydroxyapatite for water are roughly similar. Given the role of viscous resistance during absorption in a porous structure and the geometrical variability of the surface of a porous medium (solid and air alternating) we consider that the macroscopic contact angle made by a sessile drop is less relevant. The site constraint in an ultra fine capillary leads to high capillary forces dragging the liquid through the pore

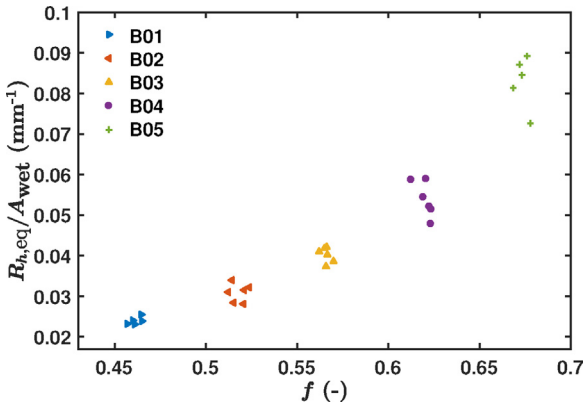

Fig. 7 – Correlation of the equivalent hydraulic radius, $R_{h,h,eq}$, and the porosity, f. $R_{h,eq}$ was estimated by fitting the LW equation (Eq. (3)) to the penetration length data from the terahertz measurements and it was normalised by the unit area exposed to the water, A_{wet}.

Table 3 – Fitting parameters and correlation performance of three different porosity-tortuosity models. More details about the models are provided in the respective reference.

Model	a (nm)	p	R^2	RMSE (nm)	Ref
Eq. (6a)	3.00	1.19	0.95	0.23	Archie (1942)
Eq. (6b)	4.53	3.52	0.96	0.22	Weissberg (1963), Comiti and Renaud (1989)
Eq. (6c)	10.57	12.33	0.96	0.21	Boudreau and Meysman (2006)

structure and therefore empirically we suggest the use of the equilibrium contact angle trending toward the receding value. This empirical interpretation is supported by the extremely rapid absorption by such fine pore networks (Ridgway et al., 2006).

The estimated $R_{h,eq}$ exhibits high consistency within each batch (see small standard deviation of $R_{h,eq}$ in Table 2) and, unsurprisingly, it is strongly correlated to the porosity (Fig. 7). The hydraulic radius ranges from 1.1 nm to 4.3 nm. The very fine size of the hydraulic radius suggests that the wicking is being driven by the finest pores at the wetting front and resisted by the permeability of the sample at long times, as described by Ridgway et al. (2006).

Besides the dependence of $R_{h,eq}$ on the porosity, it is also linked to the tortuosity (Eq. (4)). The tortuosity is again a function of the porosity (Fig. 8) and various models were proposed by other researchers to describe this relationship. We used the following three different porosity-tortuosity models (references to the models are provided in Table 3)

$$T = f^{-p} \tag{6a}$$

$$T = 1 - p \ln f \tag{6b}$$

$$T = 1 + \frac{32p}{9\pi}(1 - f), \tag{6c}$$

where p is a fitting parameter. The results for the different models are summarised in Table 3. Interestingly, the best fit ($R^2 = 0.96$) is provided by the model given in Eq. (6c), which is the only geometrical model tested. If we neglect the effect of tortuosity ($T = 1$), the coefficient of determination and RMSE drop to 0.77 and 0.38 nm, respectively. This clearly demon-

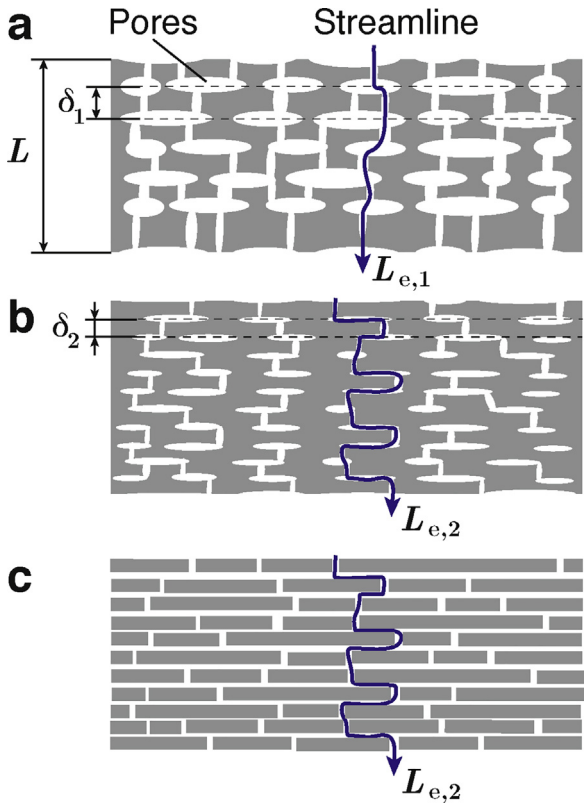

Fig. 8 – Schematic representation of the pore space in the powder compacts. Highly porous tablets (a) have shorter average lengths of the fluid path, L_e, than tablets with a lower porosity (b). The tortuosity, T, of (a) is thus smaller than that of (b). (c) is a schematic of the tortuosity-porosity model as expressed by Eq. (6c). δ is the displacement of the large anisotropic pore layers.

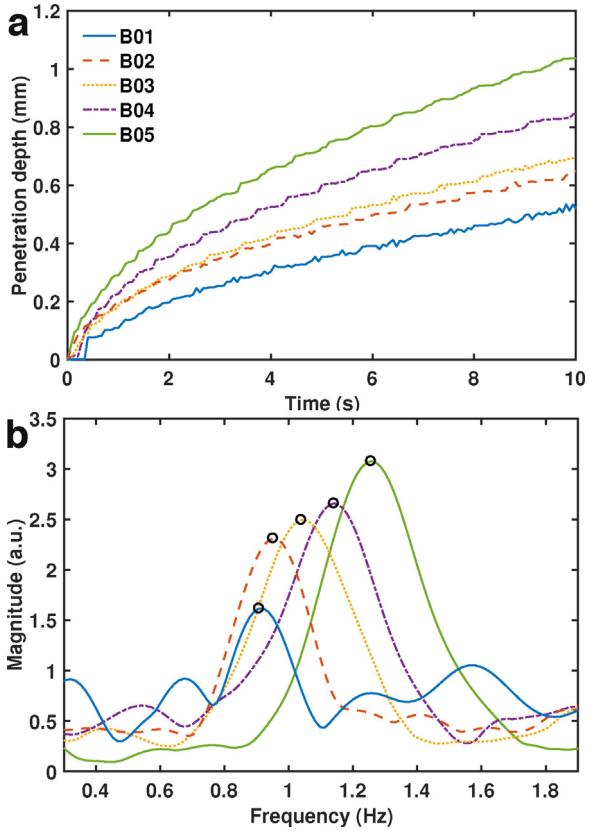

Fig. 9 – Analysis of high-frequency fluctuations of the liquid penetration data. (a) Data of one tablet per batch. (b) Batch-averaged penetration depth in frequency-domain. The open circles indicate the maximum for each batch.

strates the effect of the tortuosity on the liquid imbibition process.

Eq. (6c) was developed by Boudreau and Meysman (Boudreau and Meysman, 2006) to predict the tortuosity of muds. The model is based on the idea of the assembly of nonpenetrating and nonoverlapping blocks (disks, Fig. 8c) in order to mimic effective aggregated particles that make up the tablet. It is important to note that these blocks do not necessarily directly represent the individual particles present in the sample. The disks are aligned on a plane that is perpendicular to the direction of compaction. Moreover, the disk distribution (Fig. 8c) is obtained by taking a cross section through the actual powder compact perpendicular to the tablet face and projecting all the intersected particles onto this plane in a nonintersecting fashion. The layers of disks are separated by a small gap of constant width, which is large compared to the size of the water molecules penetrating into the compact. The tortuosity decreases monotonically with increasing porosity and it ranges from 8.6 ($f = 0.46$) to 5.5 ($f = 0.68$). These values are very large, which is attributed to the fact that these tortuosity values account for the "true" tortuosity as well as the so-called constrictivity of the pores (Boudreau, 1996).

The fitting of Eq. (4) combined with Eq. (6c) to the estimated $R_{h,eq}$ yielded a value of $p = 12.33$, where p is defined as the radius to thickness ratio of the disks. The high p value indicates that the disks must be larger in diameter than thickness, which suggests a strongly anisotropic structure. This is in excellent agreement with the results reported by Markl et al. (2017b), which revealed that the pore space is dominated by anisotropic inter-particle pores with their principal axes perpendicular to the tablet faces. We want to emphasise that the tortuosity in the radial direction is not necessarily the same as that in the axial direction. Our discussion is restricted to only one value of the tensor-tortuosity.

3.2. *Fluctuations of moving liquid front*

The high acquisition rate (15 Hz) facilitates the analysis of rapid movements of the water front. The penetration length data feature fluctuation superimposing the t- and $\sqrt{t}$-dependent behaviour (Fig. 9a). These fluctuations were analysed on the basis of the frequency-domain data of the penetration depth. Zero padding and a Hann window were applied to increase the number of frequency bins and to reduce side lobes. We analysed only the penetration data in the range of 4–12 s as the fluctuations were more pronounced in this time span. The frequency and magnitude of the fluctuations become larger with increasing porosity (Figs. 9b and 10). In particular the oscillation frequency is strongly correlated with the porosity ($R^2 = 0.9$, Fig. 10a). We performed an additional experiment including a flow dampener in order to assure that the observed fluctuations are not an effect of the peristaltic pump. The additional measurement is in excellent agreement with the results reported here and it therefore clearly indicates that the observed oscillations depend on the tablet structure rather than on the pulsation of the inlet flow.

These findings reinforce the need to consider anisotropic shape of pores and it further reveals that there are larger building blocks which have a low permeability. The liquid thus

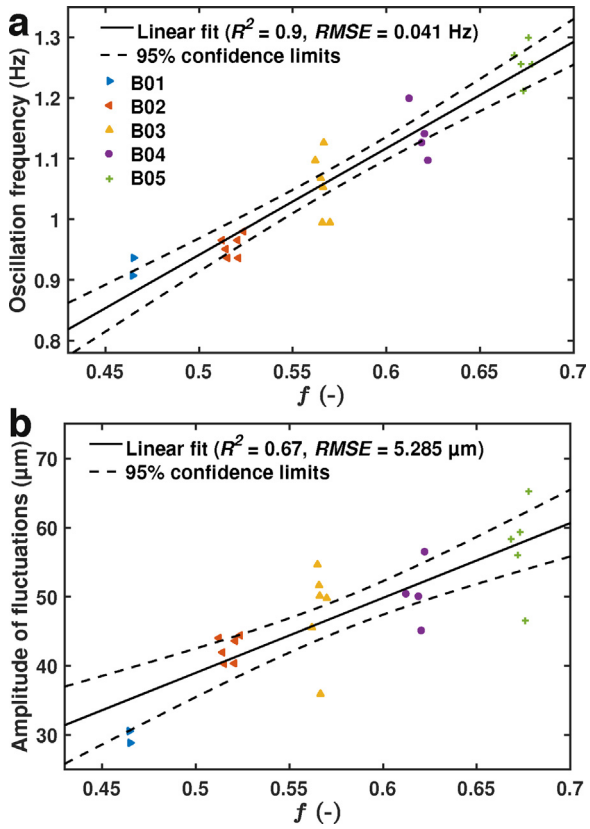

Fig. 10 – Correlation of the fluctuations with the porosity. (a) Oscillation frequency and (b) amplitude of single measurements as a function of the porosity. These fluctuations could not been detected for 3 measurements of B01 and for 2 measurements of B04.

by-passes these blocks of FCC particles and travels through a throat to the next large pore (see Fig. 8a). This by-passing, however, is presumably driven by surface film flow as otherwise the inertial retardation of the large volume flow in the interagglomerate pore space would slow the imbibition. This surmise would be consistent with the observably very fine equivalent hydraulic radius. A change in pore diameter along the streamlines is typically reflected by a constrictivity factor as discussed above. These fluctuations thus support the assumption above that the tortuosity in Eq. (4) incorporates both the "true" tortuosity and the constrictivity. The pore channels thus constrict and expand leading to variations in fluid velocity and thus the likelihood of film flow occurring when inertial retardation becomes high.

Furthermore, the displacement of the large anisotropic pore layers (δ in Fig. 8a and b) increases with increasing porosity. The fluctuations are less pronounced for low porosity tablets which is attributed to the lower anisotropy of the pores.

4. Conclusion

This study has successfully demonstrated the use of TPI to resolve the rapid liquid imbibition of highly porous FCC tablets. Effective disintegration of a pharmaceutical tablet is critical in ensuring high exposure times of the API to physiological fluids, so that the API is absorbed in greater amounts and at higher rates, leading to a faster onset of the desired pharmacological effect. By monitoring disintegration phenomena on a real-time basis, a deeper understanding of the underlying mechanisms and factors can be achieved.

Given that FCC is practically insoluble in water and does not swell, this study provides a useful metric of how more complex pharmaceutical formulations based on FCC are likely to perform. The TPI method has proven clear potential to be a technology platform for the measurement and quantification of rapid disintegration processes such as those observed in ODT.

Acknowledgements

We would like to thank Omya International AG for providing the FCC powder and sharing their valuable experience and advice. D.M. and J.A.Z. would like to acknowledge the U.K. Engineering and Physical Sciences Research Council (EPSRC) for funding (EP/L019922/1). Additional data related to this publication are available at the Cambridge University repository (https://doi.org/10.17863/CAM.17255).

Appendix A. Hydraulic radius–tortuosity relation

The surface area of the pores, S, and the solid volume, V, as a function of the hydraulic radius, R_h, can be expressed as

$$S = 2\pi R_h n L_e = \frac{2f A_{wet} L_e}{R_h}$$

$$V = (1-f) A_{wet} L$$

with $n\pi R_h^2 \equiv f A_{wet}$. n, L, L_e, f and A_{wet} are the number of capillaries, the tablet thickness, the average length of the fluid path, the porosity and the wetted surface area, respectively. The specific surface area can then be defined as

$$S_v = \frac{S}{V} = \frac{2f}{(1-f)R_h}\frac{L_e}{L}.$$

The volume surface area of the pores is modified to

$$S_{eff} = \frac{2f A_{wet} L}{R_{h,eq}}$$

using the equivalent hydraulic radius, $R_{h,eq}$.

R_h can be related to $R_{h,eq}$ by considering a constant specific surface area:

$$\begin{aligned} S_{v,eff} &= S_v \\ \frac{2f}{(1-f)R_{h,eq}} &= \frac{2f}{(1-f)R_h}\frac{L_e}{L} \\ R_{h,eq} &= R_h \frac{L}{L_e} = R_h T^{-1}, \end{aligned} \tag{A.1}$$

where T is the tortuosity.

References

Archie, G.E., 1942. The electrical resistivity log as an aid in determining some reservoir characteristics. Trans. AIME 146, 54–62.

Bawuah, P., Tan, N., Tweneboah, S.N.A., Ervasti, T., Zeitler, J.A., Ketolainen, J., Peiponen, K.E., 2016. Terahertz study on porosity and mass fraction of active pharmaceutical ingredient of pharmaceutical tablets. Eur. J. Pharm. Biopharm. 105, 122–133.

Boudreau, B.P., 1996. The diffusive tortuosity of fine-grained unlithified sediments. Geochim. Cosmochim. Acta 60, 3139–3142.

Boudreau, B.P., Meysman, F.J.R., 2006. Predicted tortuosity of muds. Geology 34, 693.

Caramella, C., Colombo, P., Conte, U., Ferrari, F., Manna, A.L., Van Kamp, H.V., Bolhuis, G.K., 1986. Water uptake and disintegrating force measurements: towards a general understanding of disintegration mechanisms. Drug Dev. Ind. Pharm. 12, 1749–1766.

Catellani, P.L., Predella, P., Bellotti, A., Colombo, P., 1989. Tablet water uptake and disintegration force measurements. Int. J. Pharm. 51, 63–66.

Comiti, J., Renaud, M., 1989. A new model for determining mean structure parameters of fixed beds from pressure drop measurements: application to beds packed with parallelepipedal particles. Chem. Eng. Sci. 44, 1539–1545.

Desai, P.M., Liew, C.V., Heng, P.W.S., 2012. Understanding disintegrant action by visualization. J. Pharm. Sci. 101, 2155–2164.

Desai, P.M., Liew, C.V., Heng, P.W.S., 2016. Review of disintegrants and the disintegration phenomena. J. Pharm. Sci. 105, 2545–2555.

Eberle, V.A., Häring, A., Schoelkopf, J., Gane, P.A.C., Huwyler, J., Puchkov, M., 2015. In silico and in vitro methods to optimize the performance of experimental gastroretentive floating mini-tablets. Drug Dev. Ind. Pharm. 42, 808–817.

Eberle, V.A., Schoelkopf, J., Gane, P.A.C., Alles, R., Huwyler, J., Puchkov, M., 2014. Floating gastroretentive drug delivery systems: comparison of experimental and simulated dissolution profiles and floatation behavior. Eur. J. Pharm. Sci. 58, 34–43.

Esteban, J., Moxon, T.E., Simons, T.A.H., Bakalis, S., Fryer, P.J., 2017. Understanding and modeling the liquid uptake in porous compacted powder preparations. Langmuir 33, 7015–7027.

Hapgood, K.P., Litster, J.D., Biggs, S.R., Howes, T., 2002. Drop penetration into porous powder beds. J. Colloid Interface Sci. 253, 353–366.

Holm, R.T., 1991. Convention confusions. In: Palik, E.D. (Ed.), Handbook of Optical Constants of Solids. Academic Press, pp. 21–55.

Koivula, H., Alm, H.K., Toivakka, M., 2011. Temperature and moisture effects on wetting of calcite surfaces by offset ink constituents. Colloids Surf. A: Physicochem. Eng. Aspects 390, 105–111.

Markl, D., Sauerwein, J., Goodwin, D.J., van den Ban, S., Zeitler, J.A., 2017a. Non-destructive determination of disintegration time and dissolution in immediate release tablets by terahertz transmission measurements. Pharm. Res. 34, 1012–1022.

Markl, D., Wang, P., Ridgway, C., Karttunen, A.P., Chakraborty, M., Bawuah, P., Pääkkönen, P., Gane, P., Ketolainen, J., Peiponen, K.E., Zeitler, J.A., 2017b. Characterization of the pore structure of functionalized calcium carbonate tablets by terahertz time-domain spectroscopy and X-ray computed microtomography. J. Pharm. Sci. 106, 1586–1595.

Markl, D., Yassin, S., Wilson, D.I., Goodwin, D.J., Anderson, A., Zeitler, J.A., 2017c. Mathematical modelling of liquid transport in swelling pharmaceutical immediate release tablets. Int. J. Pharm. 526, 1–10.

Markl, D., Zeitler, J.A., 2017. A review of disintegration mechanisms and measurement techniques. Pharm. Res. 34, 890–917.

Mizuno, M., Fukunaga, K., Saito, S., Hosako, I., 2009. Analysis of calcium carbonate for differentiating between pigments using terahertz spectroscopy. J. Eur. Opt. Soc. 4, 09044.

Nakayama, A., Kuwahara, F., Sano, Y., 2007. Concept of equivalent diameter for heat and fluid flow in porous media. AIChE J. 53, 732–736.

Nguyen, T., Shen, W., Hapgood, K., 2009. Drop penetration time in heterogeneous powder beds. Chem. Eng. Sci. 64, 5210–5221.

Nogami, H., Nagai, T., Uchida, H., 1966. Studies on powdered preparations. XIV. Wetting of powder bed and disintegration time of tablet. Chem. Pharm. Bull. 14, 152–158.

Nott, K.P., 2010. Magnetic resonance imaging of tablet dissolution. Eur. J. Pharm. Biopharm. 74, 78–83.

Peppas, N., Colombo, P., 1989. Development of disintegration forces during water penetration in porous pharmaceutical systems. J. Control. Release 10, 245–250.

Pickwell, E., Cole, B.E., Fitzgerald, A.J., Wallace, V.P., Pepper, M., 2004. Simulation of terahertz pulse propagation in biological systems. Appl. Phys. Lett. 84, 2190–2192.

Preisig, D., Haid, D., Varum, F.J.O., Bravo, R., Alles, R., Huwyler, J., Puchkov, M., 2014. Drug loading into porous calcium carbonate microparticles by solvent evaporation. Eur. J. Pharm. Biopharm. 87, 548–558.

Quodbach, J., Kleinebudde, P., 2016. A critical review on tablet disintegration. Pharm. Dev. Technol. 47, 1–12.

Quodbach, J., Moussavi, A., Tammer, R., Frahm, J., Kleinebudde, P., 2014. Tablet disintegration studied by high-resolution real-time magnetic resonance imaging. J. Pharm. Sci. 103, 249–255.

Ridgway, C.J., Gane, P.A.C., Schoelkopf, J., 2006. Achieving rapid absorption and extensive liquid uptake capacity in porous structures by decoupling capillarity and permeability: nanoporous modified calcium carbonate. Transp. Porous Media 63, 239–259.

Sastry, S.V., Nyshadham, J.R., Fix, J.A., 2000. Recent technological advances in oral drug delivery – a review. Pharm. Sci. Technol. Today 3, 138–145.

Schoelkopf, J., Ridgway, C.J., Gane, P.A.C., Matthews, G.P., Spielmann, D.C., 2000. Measurement and network modeling of liquid permeation into compacted mineral blocks. J. Colloid Interface Sci. 227, 119–131.

Shin, C., 2017. Tortuosity correction of Kozeny's hydraulic diameter of a porous medium. Phys. Fluids 29, 023104.

Stirnimann, T., Atria, S., Schoelkopf, J., Gane, P.A.C., Alles, R., Huwyler, J., Puchkov, M., 2014. Compaction of functionalized calcium carbonate, a porous and crystalline microparticulate material with a lamellar surface. Int. J. Pharm. 466, 266–275.

Stirnimann, T., Di Maiuta, N., Gerard, D.E., Alles, R., Huwyler, J., Puchkov, M., 2013. Functionalized calcium carbonate as a novel pharmaceutical excipient for the preparation of orally dispersible tablets. Pharm. Res. 30, 1915–1925.

Tritt-Goc, J., Kowalczuk, J., 2002. In situ, real time observation of the disintegration of paracetamol tablets in aqueous solution by magnetic resonance imaging. Eur. J. Pharm. Sci. 15, 341–346.

Wagner-Hattler, L., Wyss, K., Schoelkopf, J., Huwyler, J., Puchkov, M., 2017. In vitro characterization and mouthfeel study of functionalized calcium carbonate in orally disintegrating tablets. Int. J. Pharm.

Weissberg, H.L., 1963. Effective diffusion coefficient in porous media. J. Appl. Phys. 34, 2636–2639.

Wildenschild, D., Sheppard, A.P., 2013. X-ray imaging and analysis techniques for quantifying pore-scale structure and processes in subsurface porous medium systems. Adv. Water Resour. 51, 217–246.

Yassin, S., Goodwin, D.J., Anderson, A., Sibik, J., Wilson, D.I., Gladden, L.F., Zeitler, J.A., 2015. The disintegration process in microcrystalline cellulose based tablets, Part 1: Influence of temperature, porosity and superdisintegrants. J. Pharm. Sci. 104, 3440–3450.